

Preprint of:

"EUV Spectroscopy of Xenon Ions Created Using an Electron Beam Ion Trap", in *Opto-Ireland 2005: Optical Sensing and Spectroscopy*, Proc. of SPIE Vol. 5826, K. Fahy, E. Sokell, G. O'Sullivan, A. Cummings, A. Aguilar, J. D. Gillaspay, J. M. Pomeroy, and J. N. Tan, ed. by H. J. Byrne, et al. (SPIE, Bellingham, WA, 2005) p. 351-362.

EUV Spectroscopy of Xenon Ions Created Using an Electron Beam Ion Trap

K Fahy^a, E Sokell^a, G O' Sullivan^a, A Cummings^a, A. Aguilar^b, J. D. Gillaspay^b,
J. M. Pomeroy^b, J. N. Tan^b

^aDept. of Experimental Physics, University College Dublin, Ireland.

^bNational Institute of Standards and Technology, Gaithersburg, MD, USA.

ABSTRACT

Laser-produced plasma source development for Extreme Ultra Violet (EUV) lithography has concentrated on xenon, since XeXI emits at 13.5 nm, the wavelength at which the reflectivity of MoSi mirrors is centred. However it is not obvious that the required conversion efficiencies can be achieved using xenon, and tin has been identified as a strong emitter at this wavelength. The transitions responsible in tin are $4p^6 4d^n - 4p^5 4d^{n+1} + 4p^6 4d^{n-1} 4f$ occurring in a number of adjacent ion stages that merge to form an unresolved transition array (UTA). This UTA is similar to a feature that appears between 10 nm to 11 nm in xenon, which thus provides information directly relevant to tin. The present experimental studies on xenon were performed at the NIST Electron Beam Ion Trap (EBIT). EBITs were developed to perform spectroscopic studies of highly charged ions. The experiments involved changing EBIT parameters, such as the electron beam energy, so that the distribution of ion stages within the plasma changed systematically. Analysis of the corresponding EUV spectra yields information about the contribution of various ion stages to the evolution of the UTA between 10 nm – 11 nm. Previously reported data for the ion stages XeVII through to XeXI are used to identify features occurring in the EBIT spectrum. When the EBIT relative intensities are compared to those from vacuum spark sources they are found to give better agreement with the calculated gA values (statistically weighted Einstein A-coefficients).

Keywords: EUV Spectroscopy, xenon ions, EBIT

1. INTRODUCTION

The transitions responsible for the XeXI emission are $4p^6 4d^8 - 4p^6 4d^7 5p$ as shown by Churilov *et al* [1]. The microelectronics industry requires the development of a source with a conversion efficiency of 2 % into a 3 % bandwidth [2]. Xenon does not produce significant levels of debris when compared to other target materials, however it is not obvious that the required conversion efficiency can be achieved using xenon. Plasma modeling predicts that the maximum concentration of XeXI attainable in a laser-produced plasma is about 50%. In addition to this it has been shown that the maximum absorption in the low and neutral ion stages occurs near 13.5 nm [3] thus reducing the conversion efficiency. A theoretical spectrum of XeXI [4], calculated using the COWAN suite of codes [5], is shown in figure 1 depicting the $4d - 5p$ emission band at 13.5 nm but also a much stronger one near 11 nm due to $4p^6 4d^8 - (4p^5 4d^9 + 4p^6 4d^7 4f)$ transitions.

Another EUV lithography source candidate is tin, due to strong emission originating from $4p^6 4d^n - (4p^5 4d^{n+1} + 4p^6 4d^{n-1} 4f)$ transitions. These transitions occur in a range of adjacent ion stages that overlap to produce an unresolved transition array (UTA) centred near 13.5 nm [6]. This UTA is similar to a feature that occurs in xenon in the 10 nm – 11 nm region of the spectrum, therefore analysis of the UTA in xenon should provide information that can be applied to tin. Data from an Electron Beam Ion Trap (EBIT) is complimentary to that from laser-produced plasmas in that the EBIT plasma is optically thin. Analysis of the EBIT spectra yields information about the contribution of various ion stages to the UTA evolution in xenon. In order to obtain information on the ion stages present in the EBIT plasma, previously reported lines from ion stages XeVII to XeXI, obtained from a vacuum spark source, have been convolved with an appropriate instrument function and plotted along with the EBIT spectra. We also present the evolution of the UTA as a function of EBIT electron beam energy.

2. EXPERIMENT

The current experiments on xenon were carried out at the National Institute of Standards and Technology (NIST), Gaithersburg, USA, using the EBIT facility there. The EBIT is a versatile source capable of producing nearly any ion charge state [7]. It consists of a tightly focused electron beam that serves to create, trap and excite highly charged ions. The electron beam energy is tunable, thus allowing good charge state selectivity. A superconducting Helmholtz-pair magnet provides a 3 T axial magnetic field that compresses the electron beam to a radius of about 30 μm . The electron beam is accelerated through a set of three copper electrodes or drift tubes, the outer two held at a positive potential with respect to the inner one. Neutral xenon is then injected into the middle drift tube region where the ions are formed by interaction with the electron beam. The positive ions are then trapped by a combination of the negative space charge of the electron beam, the potential well formed by the drift tubes, and the axial magnetic field.

After collisional excitation with the electron beam the radiation emitted from the plasma is viewed through a side window orientated at 90 degrees to the electron beam direction. At the NIST EBIT facility a flat – field EUV spectrometer has been built [8], based on the design of Kita et al [9]. This instrument has very efficient light gathering capability while maintaining a high resolution. The EUV spectrometer was employed in this work to obtain spectra of xenon in the 4 nm – 20 nm range. The resolution of the spectrometer varies from 0.02 nm at 4nm to 0.035 nm at 20 nm and has a wavelength accuracy of 0.02 nm across the spectral range. The detector used was a liquid nitrogen cooled, back-illuminated CCD consisting of an array of 1340 (horizontal) x 400 (vertical) pixels, operated in the spectroscopy mode. The spectroscopy mode allows binning of the 400 vertical pixels into a one – dimensional row of 1340 pixels, resulting in improved signal to noise ratios.

For different trap voltages, xenon gas was injected at a range of pressures (1×10^{-4} to 7×10^{-5} hPa, the gas pressure in the trap region being considerably lower than these values, and spectra were obtained for a range of electron beam energies. The spectra were corrected for cosmic events in post acquisition and typical integration times ranged from 3 min – 30 min.

3. RESULTS

3.1 XeVII to XeX

We present spectra obtained from the EBIT at various electron beam energies and identify some lines based on previously reported data for the ion stages XeVII to XeX. Figure 2 shows a spectrum obtained at a beam energy of 180 eV and gas injection pressure of 1.2×10^{-4} hPa (9×10^{-5} torr). At this beam energy the maximum obtainable charge state is XeX and the strongest spectral feature observed in the 4 nm – 20 nm region is the XeIX $4d^{10}^1S_0 - 4d^94f^1P_1$ transition at 12.02 nm. This line has been fitted with a Gaussian function with a full width at half maximum of 0.027 nm thus giving a measure of the instrument resolution at this wavelength. This is consistent with the instrument resolution quoted above. Convolving the data obtained by other authors with the Gaussian function just described, and superimposing the convolved data on the EBIT spectrum we have identified a number of spectral features. Similar data has been obtained for XeVII from Churilov and Joshi [10] where their data was supplemented by a set of xenon spectrograms in the 10 nm - 60 nm region [11], obtained using a gas-puff triggered spark as a source. Resonance transitions of XeVIII have earlier been identified by Kaufmann and Sugar [12] and Churilov and Joshi [13], the latter having also classified lines in XeIX and X. All of the above data is based on spectra produced using a high-voltage spark discharge. Figure 3 shows the EBIT spectrum at a beam energy of 180 eV, with the vacuum spark data superimposed for comparison. The intensity is arbitrary, with the EBIT spectrum scaled from 1 - 100 based on the strongest feature in the spectrum, the XeIX line at 12.02 nm. The vacuum spark intensities are those obtained from the literature, measured from plate darkening and scaled from 1 - 100. The line intensities from the alternative plasma sources, EBIT and spark discharge, cannot be compared absolutely but the relative intensities can be compared from the plots. Table 1 summarizes the line identifications for each ion stage under the following headings: the wavelength values, λ_{ref} , obtained from [10] – [13], the values as measured in the current work, λ_{ebit} , the identified transition, and the calculated gA values (statistically weighted Einstein A-coefficients) from the literature where this is available. In the case where spectral features were too close to be resolved in the EBIT spectra, the vacuum spark data has been summed and prominent peaks are compared. We have identified most of the strong features occurring in the EBIT spectrum at 180 eV.

3.1.1 XeVII

The analysis of Churilov and Joshi [10] reveals three prominent lines in the 4 nm – 20 nm region, and these are shown in figure 3, superimposed on the EBIT spectrum at 180 eV. The $4d^{10}5s^2\ ^1S_0 - 4d^95s^25p\ ^1P_1$ line reported at 18.5438 nm is clearly seen in the EBIT spectrum at a wavelength of 18.56 nm. The prominent peak seen in the EBIT spectrum at a wavelength of 12.34 nm coincides with the $4d^{10}5s^2\ ^1S_0 - 4d^95s^24f\ ^1P_1$ line at 12.3242 nm but also with a XeVIII double line unresolved in our spectrum. The prominent $4d^{10}5s^2\ ^1S_0 - 4d^95s^25p\ ^3D_1$ line observed in the gas-puff spectrum at 18.1876 nm is absent in the EBIT spectrum. The gA values for the transitions, as calculated by Churilov and Joshi, are shown in table 1.

3.1.2 XeVIII

The vacuum spark lines can be seen superimposed on the EBIT spectrum in figure 3. The double line due to the $4d^{10}5s^2\ ^2S_{1/2} - 4d^95s4f^2\ ^2P_{1/2,3/2}$ transitions at 12.3265 nm and 12.3243 nm respectively is unresolved in the EBIT spectrum. The convolved lines match the feature at 12.34 nm in our spectrum. The lines of the $4d^{10}5s - 4d^95s5p$ transition array are also shown with three of the reported lines in good agreement with the EBIT features at 17.09 nm, 17.73 nm and 17.79 nm.

3.1.3 XeIX

The strongest of the XeIX $4d^{10}\ ^1S_0 - 4d^9nl$ transitions occurring in both the EBIT and vacuum spark spectra is the $^1S_0 - 4f\ ^1P_1$ transition reported at 12.0133 nm and measured here at 12.02 nm. Other prominent features in both spectra are the $-5f\ ^1P_1$, $-5p^3D_1$ and $-5p^1P_1$ transitions reported at 9.6449 nm, 16.1742 nm and 16.5323 nm respectively. The reported features at 10.2815 nm ($-6p^1P_1$), 10.3808 nm ($-6p^3P_1$) and 14.3614 nm ($-4f^3D_1$) appear only very weakly in the EBIT spectrum, relative to the $^1S_0 - 4f^1P_1$ line at 12.02 nm.

3.1.4 XeX

The convolved data of Churilov and Joshi [13] for the $4p^64d^9 - (4p^64d^85p + 4p^64d^84f + 4p^54d^{10})$ transition arrays of XeX is shown in figure 3. The bulk of the emission is concentrated in two energy bands 11 nm - 12 nm (4d - 4f transitions) and 14 nm - 16 nm (mainly 4d - 5p). The prominent features of the 4d - 4f transitions in the 11 nm - 12 nm band in the EBIT spectrum match well with the reported data. The EBIT emission in the 11 nm - 12 nm band is also about a factor of 10 greater than that in the 14 nm - 16 nm band, contrary to that of the vacuum spark where the emission in the longer wavelength region is greatest. If one compares the relative gA values of the two regions these are seen to be more consistent with the EBIT intensities. When the EBIT intensities are rescaled to match the vacuum spark data in the 14 nm - 16 nm region, we observe many features common to both spectra and these are tabulated in Table 2 along with the summed gA values.

3.2 XeXI

High resolution spectra have been recorded by Churilov *et al* [14] using a low inductance triggered spark in the 10 nm - 15 nm region of the spectrum. Again this data has been convolved with a Gaussian function of FWHM 0.027 nm and superimposed on the EBIT spectrum. The spectrum obtained from the EBIT at a beam energy of 210 eV is shown in figure 3. This energy is above the ionization threshold of XeX but below that of XeXI. Thus we expect to see the 4d - 4f and 4d - 5p transition arrays of XeXI, as depicted in figure 1, feature prominently at this energy when compared to the spectrum taken at 180 eV. The spectra obtained at both 180 eV and 210 eV are shown in figure 4. Clearly the XeXI features are absent in the lower energy spectrum. However the prominent features of the XeXI $4p^64d^8 - (4p^64d^75p + 4p^64d^74f + 4p^54d^9)$ transition array are clearly visible in the EBIT spectrum at 210 eV, where the ionization threshold for XeXI production has been crossed. As with XeX, the 4d - 4f transitions, centred near 11 nm, appear considerably stronger than the 4d - 5p transitions centred near 13.5 nm, in contrast to the vacuum spark spectra. Again the EBIT relative intensities of the 4d - 4f and 4d - 5p transitions follow more closely those predicted by gA calculations as can be seen by comparing the experimental spectra with the theoretical plot in figure 1.

We have scaled the EBIT spectrum to match the vacuum spark spectrum to allow the comparison of spectral features in both the 11 nm and 13.5 nm regions. Table 3 lists the wavelengths and summed gA values of prominent peaks common to both EBIT and vacuum spark spectra.

3.3 UTA evolution and in-band ratio's

It has already been stated that the semiconductor industry requires a conversion efficiency of 3 % within a 2 % bandwidth. The emission from the 13.5 nm band, arising from the 4d - 5p transitions in XeXI, has been compared with the 4d - 4f emission from the same bandwidth centred near 11.2 nm, from the same ion stage. If the electron beam energy is increased beyond 210 eV, we start to see some features emerge between 10.5 nm and 11 nm. This is the UTA and is equivalent to that occurring near 13.5 nm in tin. A plot of the xenon UTA as a function of beam energy is shown in figure 5, for beam energies 180 eV through to 500 eV where the highest ion stage obtainable is XeXIX. The vertical axis is scaled to match the XeXI feature at 11.2 nm occurring in the EBIT spectra. The in-band ratio's are shown in figure 6 as a function of beam energy and have previously been reported by Fahy *et al* [4]. The ratio's are found for both the UTA and XeXI 4d - 4f bands, by dividing the total counts within these bands successively by the total counts falling within the band centred on the XeXI 4d - 5p emission.

4. CONCLUSION

Xenon spectra acquired at the NIST Electron Beam Ion Trap have been presented. We have focused on the spectra obtained at low electron beam energies where the ion stages relevant to the EUV lithography process are dominant. In order to infer the ion stages present in the trap at these energies, we have compared prominent features in the EBIT spectrum to those previously identified by other researchers. This data was acquired with a vacuum spark discharge as the source. The spectrum taken at 180 eV shows many of these previously identified features from XeVII through to XeX. The presence of XeXI is clearly identifiable as the ionization potential is exceeded at a beam energy of 210 eV. Clearly the relative intensities of lines obtained from these two sources can differ greatly. This is most pronounced for the 4d - 4f and 4d - 5p transitions of XeX and XI, where the EBIT favors the 4d - 4f emission over the 4d - 5p, whereas the spark discharge emits more strongly in the 4d - 5p region. When the relative intensities from the two alternative plasma sources are compared to the theoretical gA values, it seems that the EBIT relative intensities are closer to the theoretical ones than those obtained from the spark discharge source, perhaps because the EBIT is a low density continuous light source. The in-band ratio's relevant to EUV lithography development have been shown previously [4] and are included here for completeness. The UTA, equivalent to the feature occurring at around 13.5 nm in tin, is seen to evolve as a function of beam energy as higher ion stages contribute. Work is currently underway to extend the current analysis to a full parameterization of the UTA.

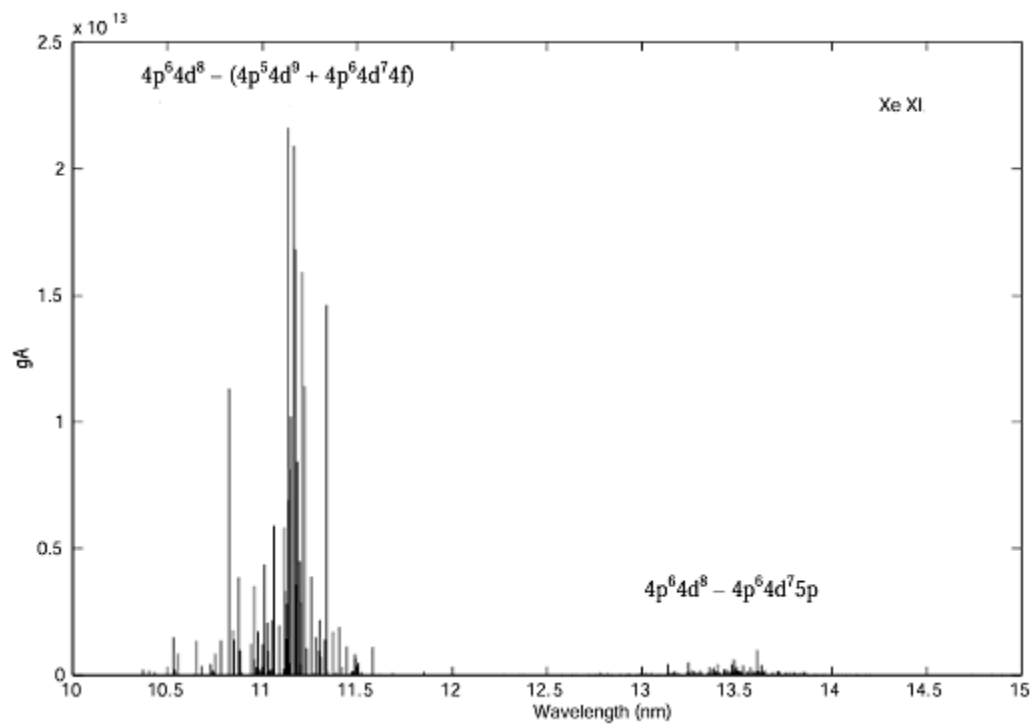


Figure 1: Theoretical spectrum for XeXI.

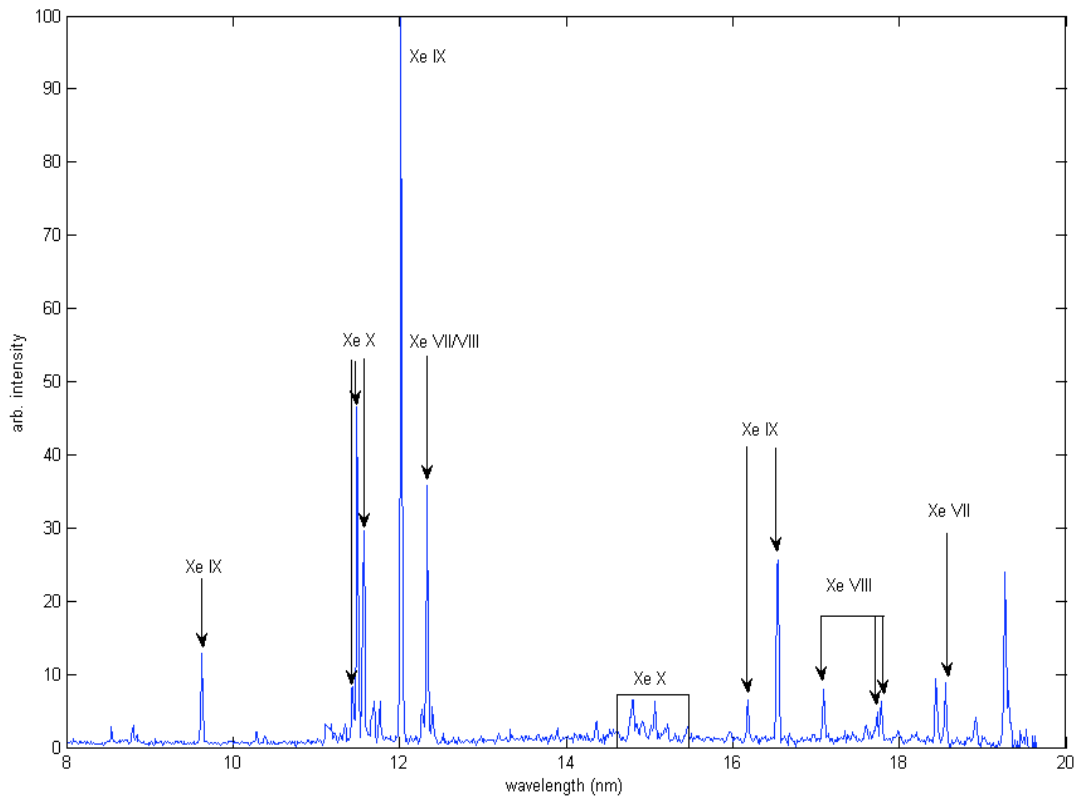


Figure 2: EBIT spectrum taken at 180 eV electron beam energy and a gas injection pressure of 1.2×10^{-4} hPa (9×10^{-5} torr). This energy is just below that required to obtain XeXI. The spectral features visible in the above spectrum are due to emission from XeVII, VIII, IX and X ion stages.

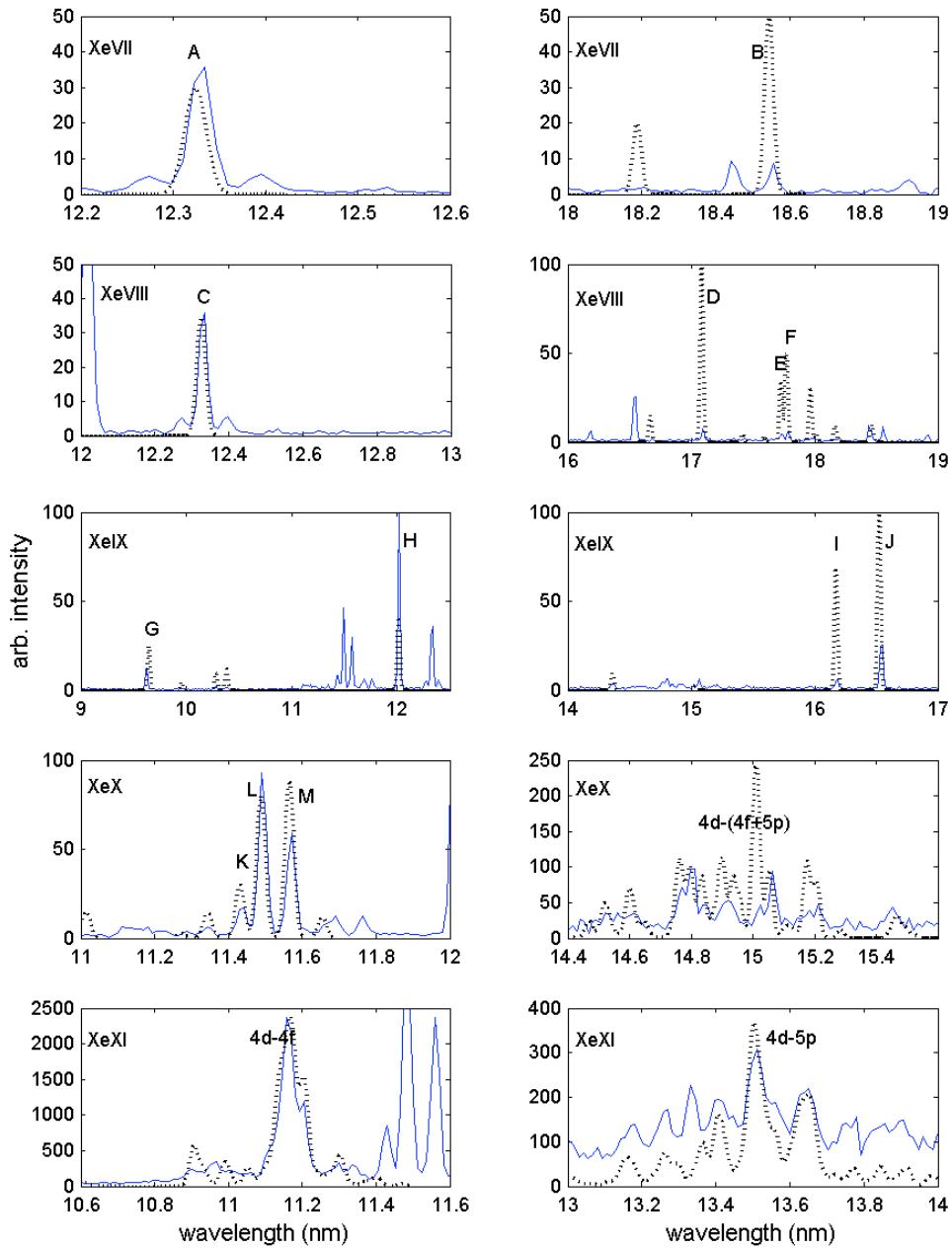


Figure 3: EBIT spectra at 180 eV and 210 eV showing features from the ion stages XeVII to XeXI. The identified features are labeled above and listed in Tables 1-3. In the case of the XeX and XeXI transition arrays the EBIT data (solid line) has been rescaled to enable comparison with the vacuum spark data (dashed line).

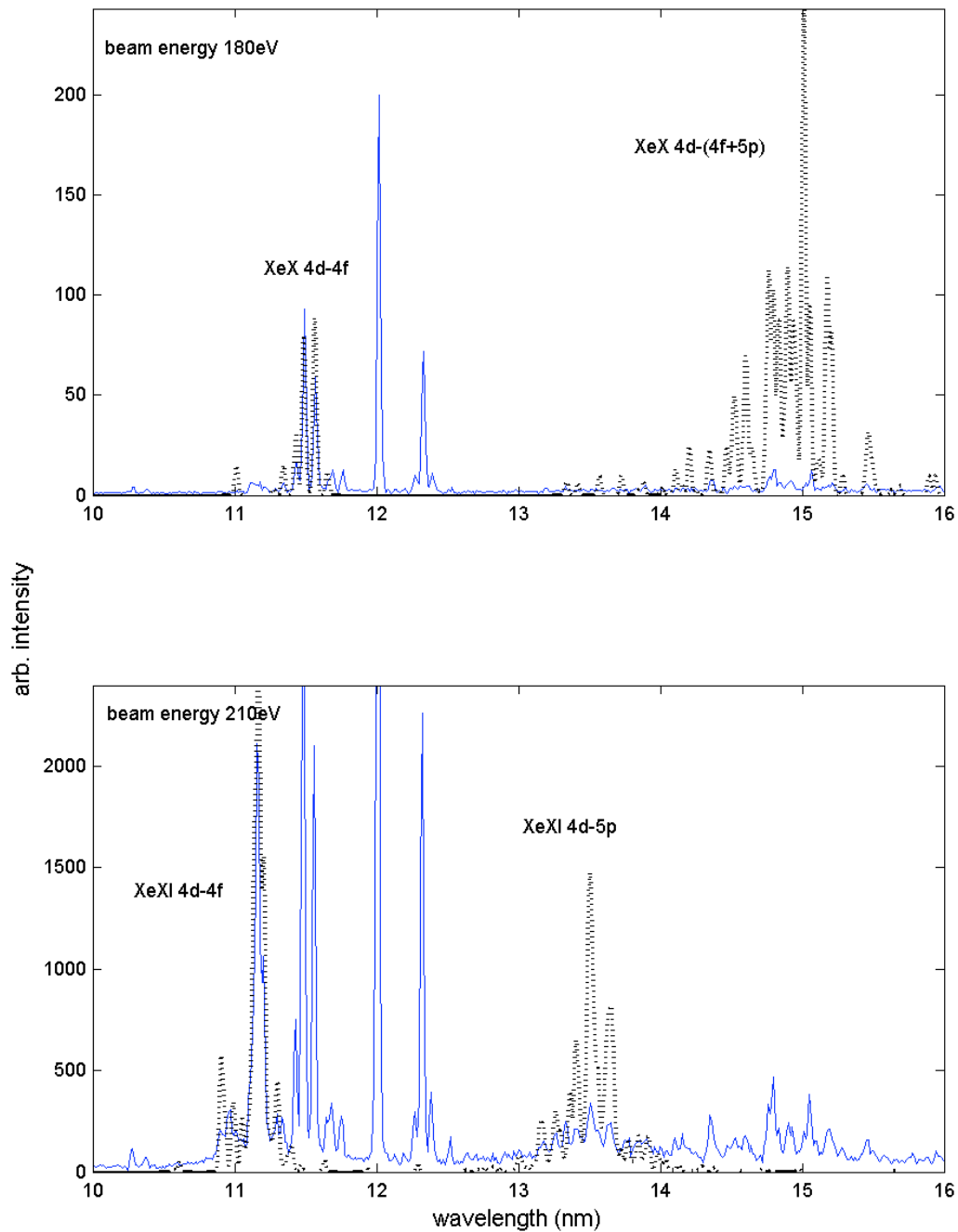


Figure 4: EBIT spectra obtained with an electron beam energy of 180 eV and 210 eV respectively. The vacuum spark data (dashed line) is seen convolved on the EBIT data (solid line) in both cases. The spectrum at 210 eV clearly shows the XeXI 4d - 4f and 4d - 5p transitions that are absent in the lower energy spectrum.

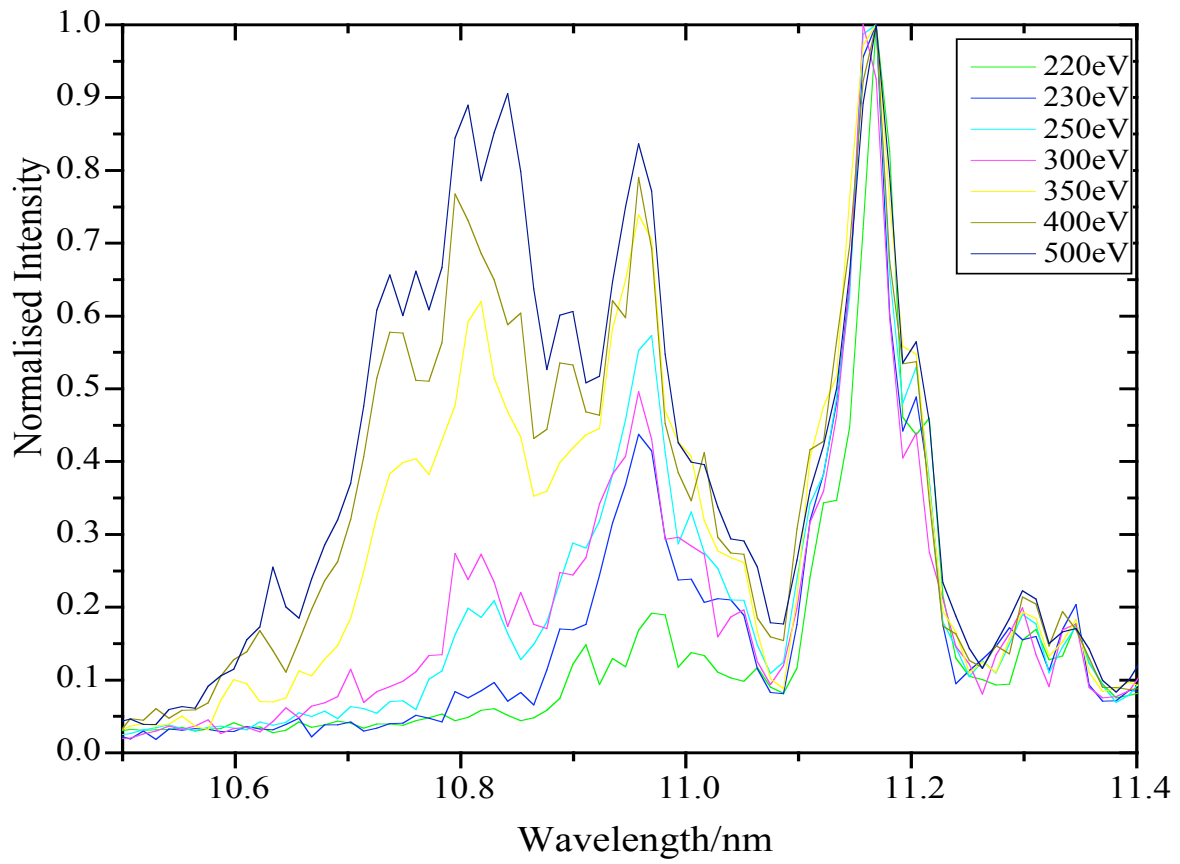


Figure 5: UTA evolution with electron beam energy. The vertical axis has been scaled to match the intensity of the XeXI feature occurring at 11.2 nm.

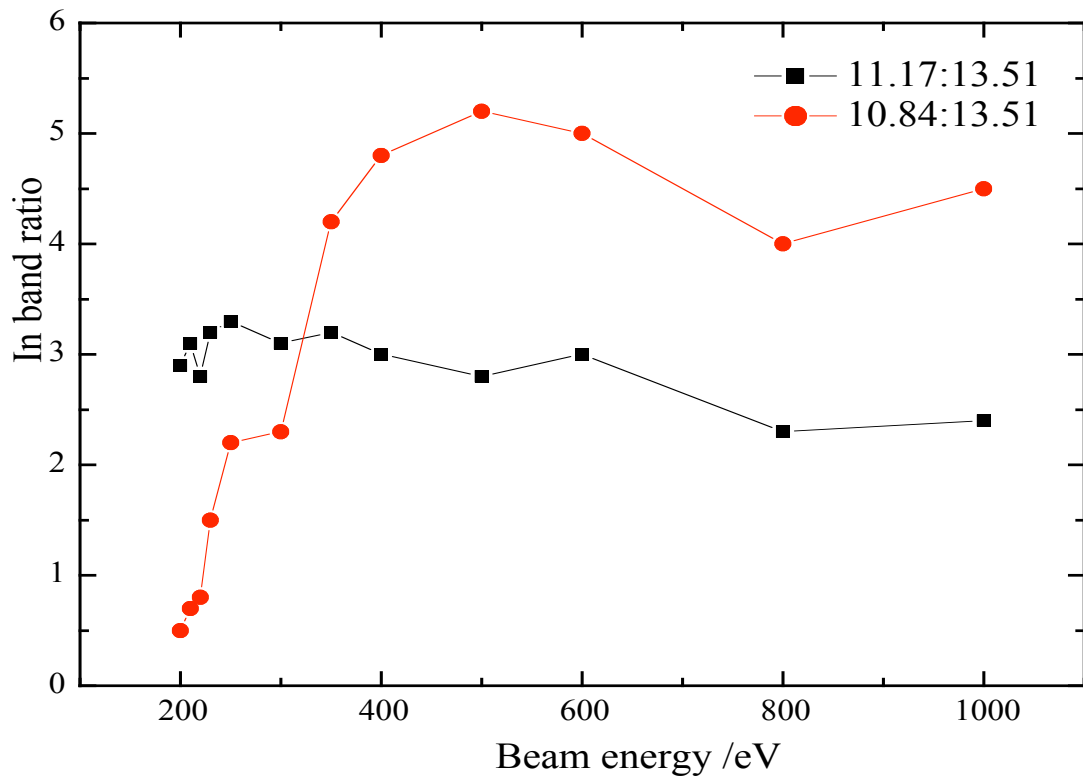


Figure 6: In band ratios as a function of EBIT beam energy. The ratios were obtained by dividing the number of counts in a 0.27 nm band centred at 11.17 nm (squares) and 10.84 nm (circles) by the counts in a similar band centred at 13.51 nm.

Label	Ion	_ref	_ebit	Transition	gA (x10 ⁹ s ⁻¹)	Ref
A	XeVII	12.3242*	12.34	5s ² 1S ₀ - 4d ⁹ 5s ² 4f ¹ P ₁	6645	10
B		18.5438	18.56	5s ² 1S ₀ - 4d ⁹ 5s ² 5p ¹ P ₁	222.5	10
C	XeVIII	12.326**	12.34	5s ² S _{1/2} - 4d ⁹ 5s4f ² P _{1/2} 5s ² S _{1/2} - 4d ⁹ 5s4f ² P _{3/2}	12569**	13
D		17.0856	17.09	5s ² S _{1/2} - 4d ⁹ 5s5p (5/2, ¹ P ₁) _{3/2}	-	12
E		17.7258	17.74	5s ² S _{1/2} - 4d ⁹ 5s5p (3/2, ³ P ₁) _{1/2}	-	12
F		17.7707	17.79	5s ² S _{1/2} - 4d ⁹ 5s5p (3/2, ³ P ₁) _{3/2}	-	12
G	XeIX	9.6449	9.63	4d ¹⁰ 1S ₀ - 4d ⁹ 5f ¹ P ₁	1538	13
H		12.0133	12.02	4d ¹⁰ 1S ₀ - 4d ⁹ 4f ¹ P ₁	4554	13
I		16.1742	16.19	4d ¹⁰ 1S ₀ - 4d ⁹ 5p ³ D ₁	45	13
J		16.5323	16.55	4d ¹⁰ 1S ₀ - 4d ⁹ 5p ¹ P ₁	241	13
K	XeX	11.4312	11.43	4p ⁶ 4d ⁹ 2D _{5/2} - 4f(874794) _{3/2}	4942	13
L		11.4880	11.49	4p ⁶ 4d ⁹ 2D _{5/2} - 4f(870470) _{7/2}	14400	13
M		11.5661	11.57	4p ⁶ 4d ⁹ 2D _{5/2} - 4f(864592) _{5/2}	9796	13

Table 1: Table showing identification of lines from the EBIT spectra, based on comparison with vacuum spark data.

* This line coincides with the XeVIII double line.

** This is a double line that is unresolved in the EBIT spectrum. The reference wavelength and gA values are those obtained when the double line is convolved with a Gaussian of full width at half maximum of 0.027 nm.

_ref	_ebit	Summed gA (x10 ⁹ s ⁻¹)
14.764	14.77	307
14.798	14.80	320
14.834	14.84	191
15.010	15.02	312
15.054	15.06	248
15.176	15.18	129
15.206	15.21	113

Table 2: Table showing the prominent features of the XeX 4p⁶4d⁹ - (4p⁶4d⁸5p + 4p⁶4d⁸4f + 4p⁵4d¹⁰) transition array occurring in the EBIT spectrum at 180 eV beam energy. The high resolution data of [13] has been convolved with a Gaussian function for comparison (see figures 3 and 4) and the summed gA values are listed in column 3 above.

<u>_ref</u>	<u>_ebit</u>	Summed gA (x10 ⁹ s ⁻¹)
11.168	11.16	56271
11.204	11.20	35321
13.164	13.18	503
13.260	13.27	721
13.364	-	474
13.408	13.41	760
13.504	13.51	173
13.648	13.65	118

Table 3: Table showing the prominent features of the XeXI $4p^64d^8 - (4p^64d^75p + 4p^64d^74f + 4p^54d^9)$ transition array occurring in the EBIT spectrum at 210 eV beam energy. The high resolution data of [14] has been convolved with a Gaussian function for comparison (see figures 3 and 4) and the summed gA values are listed in column 3 above.

ACKNOWLEDGMENTS

This work was supported by Science Foundation Ireland under Investigator Grant **02/IN.1/199**, International SEMATECH under LITH152, and in part by the U.S. Department of Commerce.

REFERENCES

- [1] Churilov S S Joshi Y N and Reader J 2003 *Optics Letters* **28** 1478
- [2] Silverman P 2002 *Proc. 1st EUVL Symposium, Dallas*
- [3] Anderson P Anderson T Folkman F Ivanov V K Kjeldsen H and West J B 2001 *J. Phys. B: At. Mol. Opt. Phys.* **34** 2009
- [4] Fahy K *et al* 2004 *J. Phys. D: Appl. Phys.* **37** 3225-3232
- [5] Cowan R D 1991 *The Theory of Atomic Structure and Spectra* (University of California Press, Berkeley)
- [6] Mandelbaum *et al* 1987 *Physical Review A* **35** 5051
- [7] Gillaspy JD 1997 *Phys. Scr.* **T71** 99
- [8] Blagojevic B, LeBigot E-O, Aguilar A, Fahy K, Makonyi K, Takács E, Tan J N, Pomeroy J M, Burnett J H, Gillaspy J D and Roberts J R 2004 in preparation.
- [9] Kita T Harada T Nakano N and Kuroda H 1983 *Appl. Opt.* **22** 512
- [10] Churilov S S and Joshi Y N 2002 *Physica Scripta* **65** 35-39
- [11] Kaufman V and Sugar J 1987 *J. Opt. Soc. Am. B* **4** 1919
- [12] Kaufman V and Sugar J 1984 *J. Opt. Soc. Am. B* **1** 38-40
- [13] Churilov S S and Joshi Y N 2002 *Physica Scripta* **65** 40-45
- [14] Churilov S S Joshi Y N Reader J and Kildiyarova R R 2004 *Phys. Scr.* **70** 26.